Structure of the nonmigrating semidiurnal tide above Antarctica observed from the TIMED Doppler Interferometer

H. Iimura,[1,2] S. E. Palo,[1] Q. Wu,[3] T. L. Killeen,[3] S. C. Solomon,[3] and W. R. Skinner[4]

Received 13 June 2008; revised 16 February 2009; accepted 26 February 2009; published 2 June 2009.

[1] Spatial structure and temporal evolution of the nonmigrating semidiurnal tidal components over Antarctica are determined by analyzing horizontal wind measurements in the Mesosphere and Lower Thermosphere (MLT) collected using TIMED Doppler Interferometer (TIDI) on the NASA Thermosphere Ionosphere Mesosphere Energetics and Dynamics (TIMED) satellite from 2002 to 2007. The data were organized into six specific intervals of approximately 60 days corresponding to the TIMED yaw periods. The results confirm the existence of a westward propagating zonal wave number 1 (W1) semidiurnal tidal component in the Antarctic MLT meridional wind field prior to the Austral summer solstice. This wave achieves a peak amplitude near 20 m s^{-1} at 90 km and is vertically stratified while extending latitudinally from the pole to 60°S. A similar structure is observed in the zonal wind field. However, the amplitude maximizes around the Austral summer solstice during the yaw period spanning 15 November to 15 January. In addition to a strong latitudinal gradient in amplitude, the W1 component also shows a vertical wavelength from 20 km near the pole to 40 km at 60°S. The amplitude and phase agree well with ground-based meteor radar observations from the South Pole. Evidence for significant though weaker standing (S0) and W3 components is also found. These components diminish in the vicinity of the pole and appear during the winter months with latitudinally restricted structures. The vertical wavelength of the S0 component during the summer is 25 km, similar to the W1 component. During the winter the wavelength of the S0 component becomes nearly evanescent.

Citation: Iimura, H., S. E. Palo, Q. Wu, T. L. Killeen, S. C. Solomon, and W. R. Skinner (2009), Structure of the nonmigrating semidiurnal tide above Antarctica observed from the TIMED Doppler Interferometer, *J. Geophys. Res.*, *114*, D11102, doi:10.1029/2008JD010608.

1. Introduction

[2] Solar thermal tides play an important role in the dynamics of the Mesosphere and Lower Thermosphere (MLT). These tides are excited by H_2O insolation absorption of infrared radiation in the troposphere and lower stratosphere, by O_3 insolation absorption of ultraviolet radiation in the mesosphere and by O_2 absorption of UV and EUV solar radiation in the thermosphere [*Forbes*, 1995]. Comparatively little solar radiation is absorbed in the MLT [*Forbes*, 1995], and therefore, in situ thermotidal forcing is expected to be either weak or absent. However, ground-based and satellite measurements of wind and temperature have revealed strong tidal signatures in the MLT [*Portnyagin et al.*, 1994; *Fritts and Isler*, 1994; *McLandress et al.*, 1994; *Burrage et al.*, 1995, and references therein]. These tides are forced from below and propagate upward, growing in amplitude as neutral atmospheric density decreases [*Chapman and Lindzen*, 1970; *Forbes and Garrett*, 1979].

[3] The tidal fields observed in the MLT are composed of a superposition of migrating tides, which propagate with the apparent motion of the solar forcing, and nonmigrating tides, which have different propagation speeds and can propagate eastward, westward, or can be standing. The nonmigrating tides are an important source of tidal variability and are believed to arise because of zonal asymmetries in the global distribution of solar irradiance absorption [*Kato et al.*, 1982] or latent heat release [*Lindzen*, 1978]. While these zonal asymmetries in tidal forcing can excite nonmigrating tides, a second mechanism involving nonlinear interactions [*Teitelbaum and Vial*, 1991] between global-scale atmospheric waves is also probably important. Nonlinear interactions between migrating and/or nonmigrating tides and stationary planetary waves can excite nonmigrating tidal components [*Teitelbaum and Vial*, 1991; *Palo et al.*, 1998]. Furthermore, in specific cases it is possible for

[1]Department of Aerospace Engineering Sciences, University of Colorado, Boulder, Colorado, USA.
[2]Now at Colorado Research Associates, Boulder, Colorado, USA.
[3]National Center for Atmospheric Research, High Latitude Observatory, Boulder, Colorado, USA.
[4]Space Physics Research Laboratory, University of Michigan, Ann Arbor, Michigan, USA.

0148-0227/09/2008JD010608

the interactions between the migrating tides and traveling planetary waves to generate nonmigrating tidal components [*Palo et al.*, 1998]. For the case of a nonlinear interaction between the migrating semidiurnal tide (W2) and a stationary planetary wave with zonal wave number 1 (SPW1), it is expected that westward propagating zonal wave number 1 (W1) and 3 (W3) semidiurnal tides will be excited. Model results from *Angelats i Coll and Forbes* [2002] have supported the supposition that a nonlinear interaction between the W2 semidiurnal tide and the SPW1 can give rise to the W1 semidiurnal tide. Explicit evidence for the existence of a W1 semidiurnal tide has been provided by meteor radar observations at the South Pole [*Forbes*, 1995; *Forbes et al.*, 1999b; *Portnyagin et al.*, 1998] which is consistent with the W1 semidiurnal tidal solution of Laplace's tidal equation [*Forbes et al.*, 1999a]. The W1 semidiurnal tide has also been observed by ground-based radar measurements at multiple stations spanning latitudes from 75°S to 78°S [*Portnyagin et al.*, 1998; *Riggin et al.*, 1999; *Baumgaertner et al.*, 2006]. At lower latitudes of 67°S to 69°S the semidiurnal tide was found to be a mixture of nonmigrating and migrating components [*Portnyagin et al.*, 1998; *Murphy et al.*, 2006].

[4] While the diurnal tide is the largest component of the tidal field in the equatorial MLT, the semidiurnal tide dominates at latitudes poleward of 40°N/S. Thus, the nonmigrating components of the semidiurnal tide are likely to be important in understanding the global-scale dynamics of the MLT. Despite efforts to determine the dominant components of the nonmigrating semidiurnal tide with ground-based instrumentation, it has proven difficult to unambiguously extract the latitudinal and altitude variations of these fields due to the limited number of measurement locations and the inherent aliasing that results. However, these difficulties can be overcome using suitable satellite measurements. The TIMED Doppler Interferometer (TIDI) on the TIMED satellite provides measurements of the horizontal winds from pole to pole in the MLT and allows assessments of the W1 semidiurnal tide within each 1200 h of local time precession of the TIMED satellite, or within each yaw period.

[5] In this paper, we present a spatial structure of the nonmigrating semidiurnal tide observed over Antarctica estimated from TIMED TIDI wind measurements. Section 2 describes the TIDI instrument, the wind measurements in the Antarctic region, and our analysis approach for determining the nonmigrating tidal components. Results from our analysis of 6 years of observations are presented in section 3. The nonmigrating semidiurnal tidal components that exhibit significant amplitudes poleward of 60°S are shown. They are the westward propagating zonal wave number 1 and 3 (W1 and W3), the standing zonal wave number 0 (S0) components. Additionally, the eastward propagating zonal wave number 1 (E1) component is also shown. These results complement the previous work of *Oberheide et al.* [2007] and *Du et al.* [2007] which focused on the TIDI observations equatorward of 45°. Finally the W1 component in the vicinity of the South Pole determined from the TIDI measurements from mid-November to mid-January is compared with ground-based meteor radar wind measurements from the South Pole. This comparison shows very good agreement, better than a few meters per second in amplitude between the TIDI and meteor radar observations, indicating that the TIDI measurements of the nonmigrating semidiurnal tide are robust.

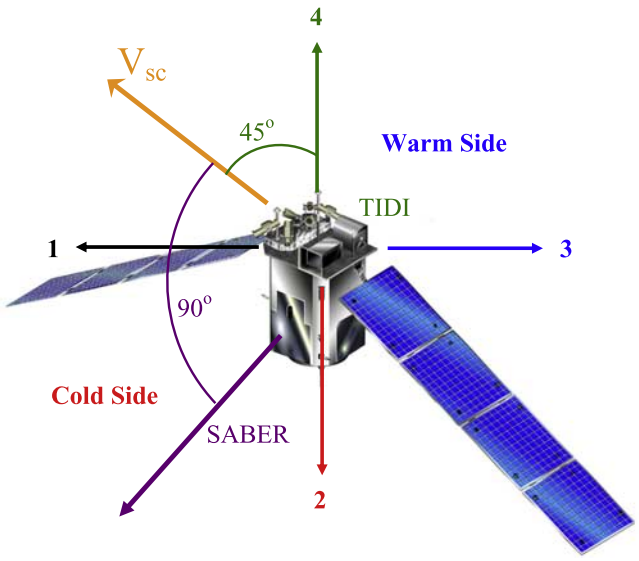

Figure 1. Image of TIMED spacecraft and viewing directions of four TIDI telescopes and SABER.

2. TIDI Measurements

[6] The Thermosphere-Ionosphere-Mesosphere Energetics and Dynamics (TIMED) spacecraft was launched in December 2001 with a mission focusing on the Earth's Mesosphere and Lower Thermosphere/Ionosphere (MLTI, 70–120 km) [*Yee et al.*, 1999]. One of the four instruments on board the TIMED satellite is the TIMED Doppler Interferometer (TIDI). The TIDI instrument is a Fabry-Perot interferometer designed to measure the vector horizontal wind and temperature fields [*Killeen et al.*, 1999, 2006]. TIDI measures horizontal wind velocities from pole to pole on every orbit over the altitude range from 70 to 120 km. The inclination of the TIMED orbit is 74.1°, and a yaw maneuver is performed approximately every 60 days to keep the Sounding of the Atmosphere using Broadband Emission Radiometry (SABER) instrument on the cold side of the spacecraft.

[7] TIDI scans through the terrestrial airglow layers with a vertical altitude resolution of 2.5 km in the MLT [*Skinner et al.*, 2003] and views O_2(0-0) P9 emissions at a wavelength of 763.78 nm. For acquisition of the P9 emission, TIDI uses a 0.3 nm narrowband filter centered at this wavelength. With two telescopes on each side of the spacecraft each at 45° and 135° angles with respect to the spacecraft's velocity vector, TIDI has the ability to measure the line-of-sight (LOS) wind velocities simultaneously in the four orthogonal directions. The two LOS measurements on each side of the spacecraft can be combined to determine the vector horizontal wind field.

[8] At high latitudes, poleward of 60°N/S, only two telescopes on one side of the spacecraft measure the LOS wind velocities. The telescopes that view the high-latitude regions alternate from the cold side to the warm side following each yaw maneuver. Figure 1 shows an image of the TIMED

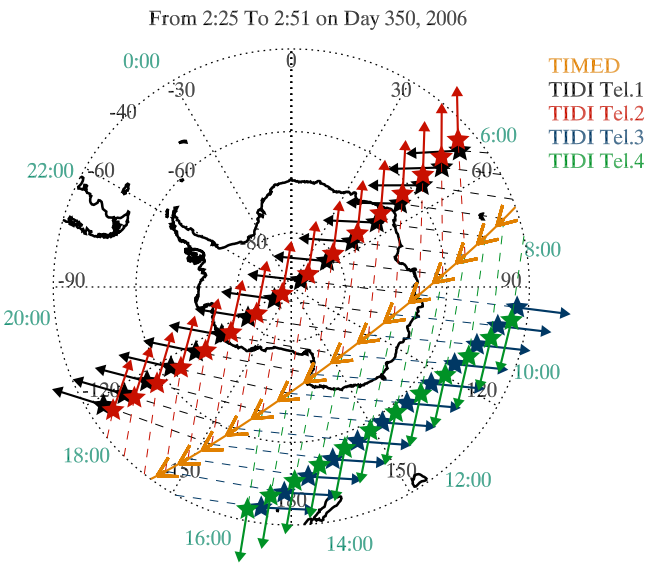

Figure 2. Trajectory of TIMED spacecraft and locations of TIDI measurements poleward of 40°S from 0225 to 0251 LT on day 350, 2006. The locations of the spacecraft at TIDI measurements are shown by yellow arrows, indicating the direction of the spacecraft. The measurement locations of the four telescopes are shown by black (telescope 1), red (telescope 2), blue (telescope 3), and green (telescope 4) stars. Arrows from the TIDI measurement locations show the viewing directions of the telescopes. Local time is indicated on the circumference.

spacecraft and indicates the location and viewing direction of the four TIDI telescopes and the SABER instrument. As the TIMED orbital plane precesses with time, the solar beta angle or Sun-orbital plane vector will change. As a result, the side of the TIMED spacecraft where the SABER instrument is located is referred to as the cold side.

[9] Figure 2 shows the trajectory of the TIMED spacecraft, in addition to the locations and viewing directions for the TIDI LOS wind measurements between 0225 and 0251 LT on day 350, 2006 poleward of 40°S. Local times are shown on the circumference. During this yaw period, the Antarctic region was being viewed from the cold side of the spacecraft. Therefore, two telescopes (telescopes 1 and 2) shown in black and red measured the LOS winds over Antarctica, and the telescopes on the other side of the spacecraft (telescopes 3 and 4) shown in blue and green did not view latitudes poleward of 60°S. During this time interval, telescopes 1 and 2 made wind measurements at local times near 0600 and 1830 LT. The location of the TIMED spacecraft when TIDI measured the horizontal wind is shown as yellow arrows indicating the direction of the spacecraft. Telescope 1 measures the LOS velocity in the forward direction while telescope 2 measures the LOS wind velocity in the rearward direction. Therefore, telescope 1 measured the LOS velocities poleward of 60°S while the spacecraft was on the descending portion of the orbit from 40°S to 74°S and the ascending portion of the orbit from 74°S to 70°S. Similarly telescope 2 measured the LOS velocities poleward of 60°S while the spacecraft was on the descending portion of the orbit from 70°S to 74°S and the ascending portion of the orbit from 74°S to 44°S.

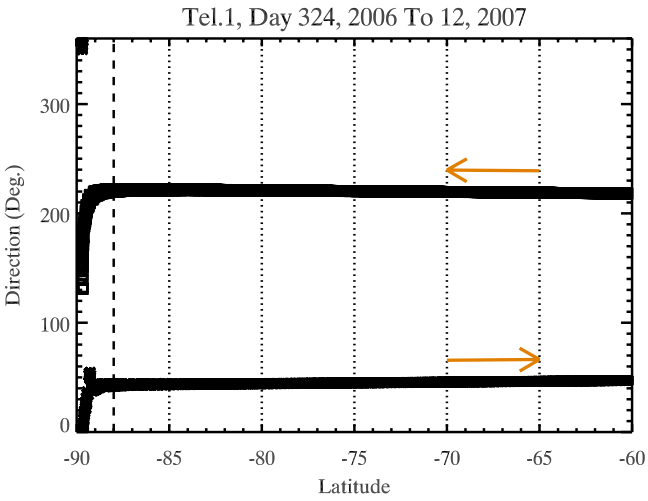

Figure 3. Line-of-sight (LOS) viewing direction for telescope 1 poleward of 60°S for the yaw period from day 324, 2006, to day 12, 2007. Arrows show the direction of the spacecraft.

[10] Figure 3 shows the LOS direction for telescope 1 poleward of 60°S during the yaw period from day 324, 2006, to day 12, 2007, which is invariant with respect to time. The angle of the LOS observing direction is defined as the angle clockwise from the north. Telescope 1 measured the LOS wind velocities along the 218° direction at 60°S and this viewing direction decreased slightly as the measurement location moved toward the pole. Poleward of 88°S the LOS viewing direction changed rapidly as the observing point moved from the descending side of the orbit to the ascending side and crossed the South Pole. On the ascending side of the orbit the viewing direction changed to 43° and increased slightly as TIDI moved northward.

[11] Figure 4 shows the local time coverage of the telescope 1 LOS measurements as a function of solar local time and longitude in the latitude band from 60°S to 65°S

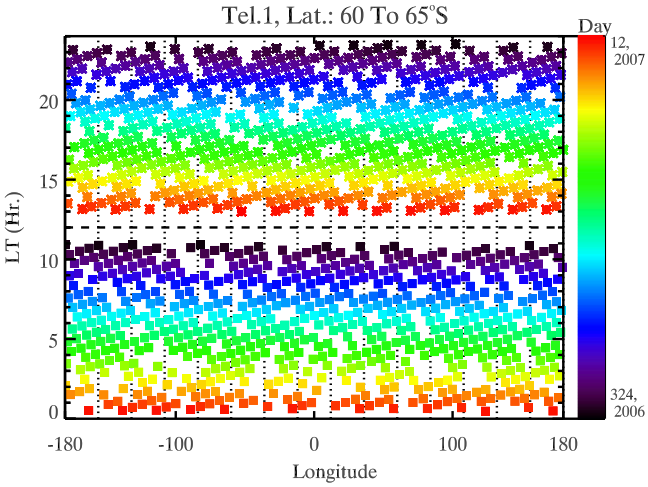

Figure 4. Local time coverage for telescope 1 in the latitude band between 60°S and 65°S for the yaw period from day 324, 2006, to day 12, 2007. Asterisks indicate ascending node data, and squares indicate descending node data.

during the yaw period from day 324, 2006, to day 12, 2007. The color of the symbols indicates the measurement day during the yaw period, while the symbols (asterisks and squares) indicate the portion of the orbit (ascending and descending). After the yaw maneuver was executed on day 324, 2006, telescope 1 measured the LOS wind velocities at local midnight during the ascending portion of the orbit and local noon during the descending portion of the orbit. Over the course of the yaw period the orbital plane precesses allowing TIDI to observe roughly 12 h of local time on the ascending portion of the orbit and 12 h of local time on the descending portion of the orbit. During this yaw period the ascending measurements covered from 2400 to 1230 LT while the descending portion of the orbit covered from 1130 to 0000 LT. There is a small measurement gap around 1200 LT due to the timing of the yaw maneuver. Other latitude bins between 60°S to 85°S and other yaw periods show similar local time coverage.

[12] Determination of systematic offsets in each of the telescope viewing directions due to the relative motion of the spacecraft, solar beta angle effects, and instrument biases can be difficult to estimate accurately [*Wu et al.*, 2006]. However, these sources of error are slowly varying and can be removed using a low-pass filter. The approach employed herein was to compute a 3-day time-longitude running mean for each altitude, latitude, and telescope separately. The observations were differenced with these means, leaving a residual time series for each telescope. The effect of removing the means from the daily measurements is to remove all slowly varying features from the observations which will include the zonal mean winds, traveling and stationary planetary waves, the migrating tides, and any systematic errors such as those described above. The migrating tides are removed in this process because they vary in local time as the satellite orbital plane precesses. The resulting residuals will contain any nonmigrating tides. Using these residuals, data were averaged into an altitude grid (2.5 km), latitude grid (5°), longitude grid (24°), and local time grid (1 h) for each yaw period and telescope separately. Data from multiple years for the same yaw period (e.g., mid-November to mid-January) were combined into a single grid for that time of year in an effort to construct a climatology. This process resulted in 6 distinct gridded data sets, one for each of the 6 yaw periods during the year. By design, the TIMED satellite is in an orbit such that the yaw maneuvers occur at nearly the same time (within 1 or 2 days) each year, allowing multiple years of data to be easily composited as described. Residuals from the two telescopes on one side of the spacecraft were then combined to compute the nonmigrating tidal components in the meridional and zonal winds from the gridded LOS measurements.

[13] The residuals from the 3-day means were used to estimate the 1-sigma confidence intervals on the estimated amplitudes and phases of the nonmigrating diurnal (24 h) and semidiurnal (12 h) tides. The estimated amplitudes and phases, which represent the times of maximum amplitude in solar local time, were fitted using a linear least squares approach. The fits were computed to the complex signals, both amplitude and phase, in longitude as a function of altitude and latitude for each yaw period. The model includes both eastward and westward propagating waves with zonal wave numbers from 1 to 6 and the standing wave. The results from this analysis provide estimates of the amplitudes and phases, where the phases are now referenced as the longitude of maximum amplitude at 0 UT, for the nonmigrating diurnal and semidiurnal tidal components. All of the results presented herein utilized the TIDI profile data version P0100_S0120_D008 produced by University of Michigan (see http://timed.hao.ucar.edu/tidi).

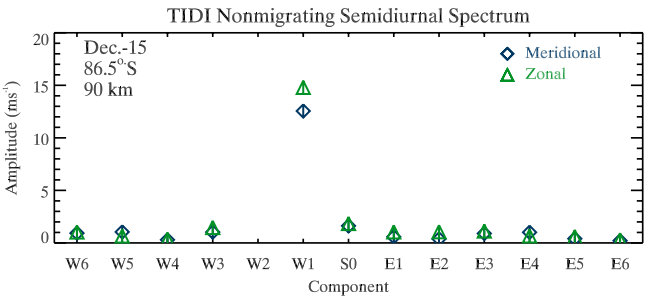

Figure 5. Amplitudes of nonmigrating semidiurnal tides from W6 to E6 at 90 km between 85°S and 88°S using all TIDI measurements in the yaw periods from mid-November to mid-January. Blue diamonds (solid line) are for the meridional component, and green triangles (dashed line) are for the zonal component.

3. Results

[14] Figure 5 shows amplitudes of the nonmigrating semidiurnal tidal components at 90 km and 86.5°S for the yaw period centered on 15 December. The nonmigrating components range from a westward propagating with the zonal wave number 6 (W6) to eastward propagating with the zonal wave number 6 (E6). The W2 component, which is migrating, does not appear in Figure 5 because the time mean and migrating tides were removed in the analysis. Figure 5 shows the dominance of the W1 component in the nonmigrating semidiurnal tidal wind field at one specific altitude, latitude, and yaw period. The meridional W1 component is 12.6 ± 0.6 m s^{-1} and the zonal W1 component is 14.8 ± 0.6 m s^{-1} while the other nonmigrating components are small in comparison with the W1 component they exhibit significant amplitudes at other latitude, altitudes, and yaw periods. The remainder of this section focuses on each of the following nonmigrating components, W1, S0, W3 and E1, showing their structure throughout the Antarctic MLT.

3.1. Westward Propagating Zonal Wave Number 1

[15] Figure 6 shows the spatial structure of the W1 component as a function of latitudes from 60°S to 86.5°S and altitudes from 80 to 110 km for the six yaw periods. The overall structure of the W1 component exhibits the maximum amplitude during late spring (15 October) and summer (15 December) near 90 km, with less significant enhancements in late winter (15 August) and late summer (15 February). During the 15 August yaw period the meridional W1 component (Figure 6a) maximizes at 100 km and 82.5°S with an amplitude of 9.6 ± 1.4 m s^{-1}, while the zonal W1 component (Figure 6b) maximizes at 85 km and 72.5°S with an amplitude of 7.9 ± 1.3 m s^{-1}.

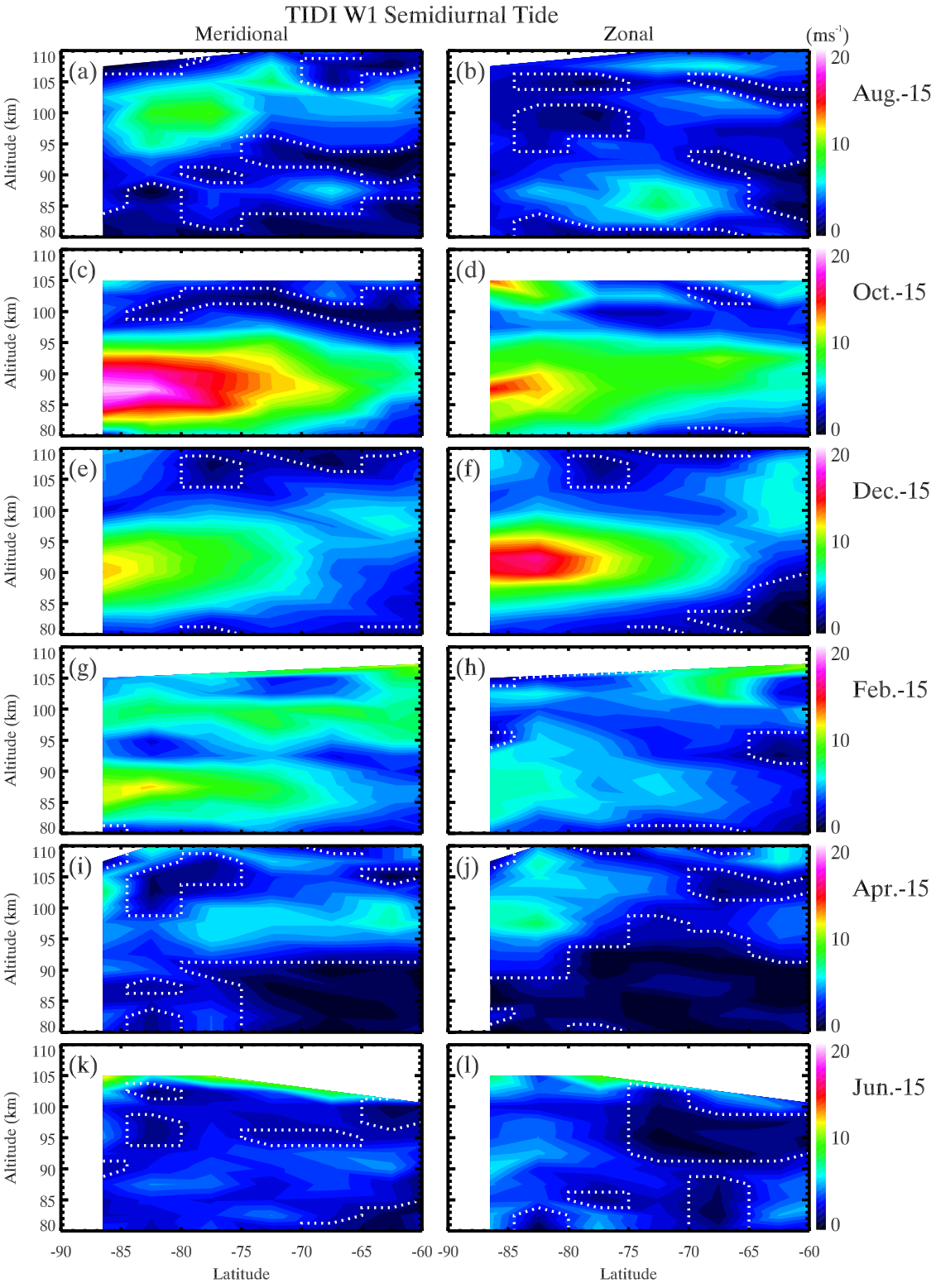

Figure 6. Spatial structure of W1 component poleward of 60°S from 80 to 110 km over six yaw periods. The component in (a, c, e, g, i, k) meridional and (b, d, f, h, j, l) zonal winds is shown. The six yaw periods are centered on 15 August, 15 October, 15 December, 15 February, 15 April, and 15 June, and run from top to bottom. Colors range from 0 (black) to 20 m s^{-1} (white). Amplitudes in a statistical 95% confidence interval are contoured by while dotted lines.

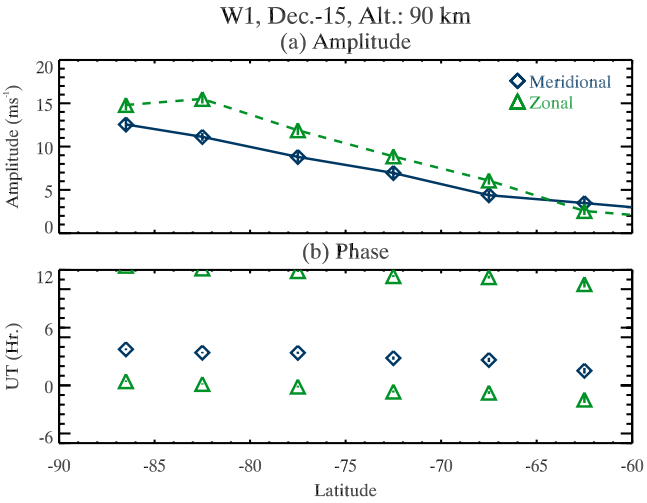

Figure 7. Latitude variations of (a) the amplitude and (b) the phase for the W1 component at 90 km from mid-November to mid-January. Blue diamonds (solid line) and green triangles (dashed line) indicate the component in the meridional and zonal winds. One-sigma confidence intervals are shown for both the amplitude and phase estimates.

Between August and October, the W1 component grows significantly and maximizes near 90 km. Additionally, during this period a clear poleward gradient is established with the amplitude increasing toward the pole. During this period the meridional amplitude exceeds the zonal amplitude. The maximum of the component during the 15 October yaw period is 20.6 ± 1.6 m s^{-1} at 87.5 km and 86.5°S in the meridional wind (Figure 6c) while 14.8 ± 1.3 m s^{-1} at 90 km and 86.5°S in the zonal wind (Figure 6d). As we move to the summer solstice, the structure of the W1 component remains largely the same with amplitudes maximizing near 90 km and increasing toward the pole. During the 15 December yaw period, a maximum amplitude of 12.6 ± 0.6 m s^{-1} in the meridional wind (Figure 6e) and 14.8 ± 0.6 m s^{-1} at 90 km and 86.5°S in the zonal wind (Figure 6f). There is also evidence of an upper altitude peak near 100 km developing at lower latitudes in both meridional and zonal winds. Moving into the late summer yaw period centered on 15 February, the peak amplitude near 90 km is maintained as 11.0 ± 1.2 m s^{-1} in the meridional wind (Figure 6g). The response near 100 km also grows in amplitude to 7.8 ± 0.5 m s^{-1}. However, the component in the zonal wind (Figure 6h) is significantly weaker at lower latitudes than during the previous yaw periods. Another clear peak appears above 100 km equatorward of 70°S. During the 15 April yaw period, the large peaks at 90 km have disappeared in both the meridional (Figure 6i) and zonal (Figure 6j) winds. Finally, during the 15 June yaw period, the W1 component does not show any significant structure in both the meridional (Figure 6k) and zonal (Figure 6l) winds.

[16] Figure 7 shows latitude variations of amplitude (Figure 7a) and phase (Figure 7b) for the W1 component at 90 km during the 15 December yaw period. At 62.5°S, the amplitudes in the zonal and meridional winds are 2.6 ± 0.5 m s^{-1} and 3.5 ± 0.5 m s^{-1}, respectively. The amplitudes increase poleward approximately linearly in both meridional and zonal winds. The amplitude in the meridional wind increases poleward with a slope of 4.0 ± 0.2 (m s^{-1})/10° and approaches 13.9 ± 0.4 m s^{-1} at the South Pole. It is apparent that for most of the region the zonal amplitude exceeds the meridional amplitude and exhibits a decrease poleward of 82.5°S. On the basis of the geometrical consideration in the vicinity of the South Pole, it is expected that the zonal and meridional winds will be equal in the region of the South Pole.

[17] The phase of the W1 component has a mean difference of 3.3 ± 0.2 h between in the meridional and zonal winds. The meridional and zonal phases are in approximate quadrature with the zonal phase leading the meridional phase, consistent with the tidal theory [*Chapman and Lindzen*, 1970] for a westward propagating global-scale wave. There is a latitudinal gradient in the phase, with the phase occurring at later times poleward. The latitude variation of the phase is 0.8 ± 0.1 h/10° in the meridional wind and 0.8 ± 0.07 h/10° in the zonal wind. Extrapolating the phase expects estimates of 4.2 ± 0.3 h in the meridional wind and 0.7 ± 0.1 h in the zonal wind at the South Pole, respectively.

[18] Figure 8 shows vertical profiles of amplitude (Figure 8a) and phase (Figure 8b) for the W1 component at 86.5°S during the 15 December yaw period. The altitude variations are very similar between the zonal and meridional components. The amplitude is larger in the zonal wind between 90 and 100 km than in the meridional wind. The meridional amplitude maximizes at 90 km with an amplitude of 12.6 ± 0.6 m s^{-1} and decreases between 90 and 100 km, whereas the zonal amplitude maximizes slightly higher at

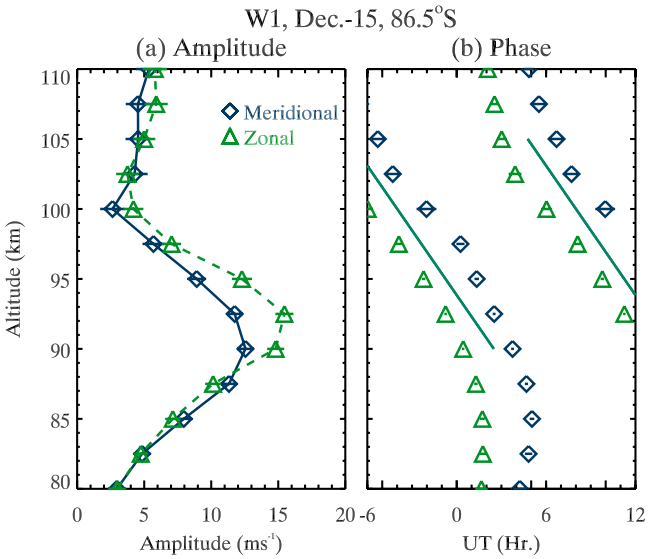

Figure 8. Altitude Variations of (a) the amplitude and (b) the phase for the W1 component between 85°S and 88°S from mid-November to mid-January. Blue diamonds (solid line) are for the meridional component, and green triangles (dashed line) are for the zonal component. One standard deviation from the mean value is shown as an error. The line shown on the phase plot indicates a mean vertical wavelength of 18.6 km.

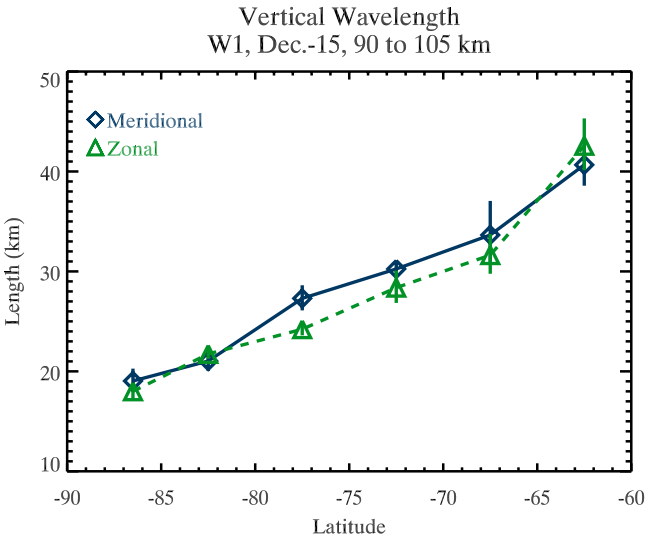

Figure 9. Latitude variation of vertical wavelength of the W1 component. The vertical wavelength is determined from a linear fit to the phase variation from 90 to 105 km. Blue diamonds (solid line) are for the meridional component, and green triangles (dashed line) are for the zonal component. One standard deviation from the mean value is shown as an error.

92.5 km with an amplitude of 15.5 ± 0.7 m s^{-1} and also decreases to 100 km. Above 100 km, the amplitude exhibits little variation with altitude. The vertical structure of the phase shows that the meridional and zonal phases are in quadrature at all altitudes with the zonal phase leading the meridional phase by nearly 3 h. Near 90 km, the phase has a transition from a very long vertical wavelength below to a much shorter wavelength above. From 90 to 105 km, the component exhibits an upward propagating structure with a vertical phase change of 0.6 ± 0.03 h km^{-1} or a vertical wavelength of approximately 19 km. Above 105 km, The phase indicates a tendency toward a longer vertical wavelength in both meridional and zonal winds.

[19] The vertical wavelengths were estimated for both winds between 90 and 105 km between 60°S and 90°S. The results from this analysis for the 15 December yaw period are shown in Figure 9. The vertical wavelength shows a consistent latitudinal trend in both meridional and zonal winds, with shorter wavelength observed at higher latitudes. This trend is nearly linear with a slope of 9 ± 0.9 km/10° and would imply a vertical wavelength of 14.5 ± 1.9 km at the South Pole.

[20] Figure 10 shows a seasonal variation of the W1 component as a function of latitude at 90 km. The W1 component maximizes between September and March in both meridional (Figure 10a) and zonal (Figure 10b) winds. The poleward increases in amplitudes are clearly visible during this period. The meridional component exhibits a maximum during the 15 October yaw period at all latitudes, while the zonal component exhibits a maximum during the 15 October yaw period at lower latitudes and during the 15 December yaw period at higher latitudes. There also appears to be narrowing in the wave response in time as one moves from higher to lower latitudes. Additionally, the meridional component appears to persist at a larger amplitude longer after the summer solstice. The minimum of the component occurs during the 15 April yaw period in both meridional and zonal winds.

3.2. Standing Zonal Wave Number 0

[21] Figure 11 is same format as Figure 6 but shows the structure of the standing zonal wave number 0 (S0) component. A clear existence of the S0 component is seen in three yaw periods centered on 15 August, 15 December, and 15 February. During these periods, the structures are very similar between the meridional and zonal winds. However, the winter structure during the 15 August yaw period is different from the summer structure during the 15 December

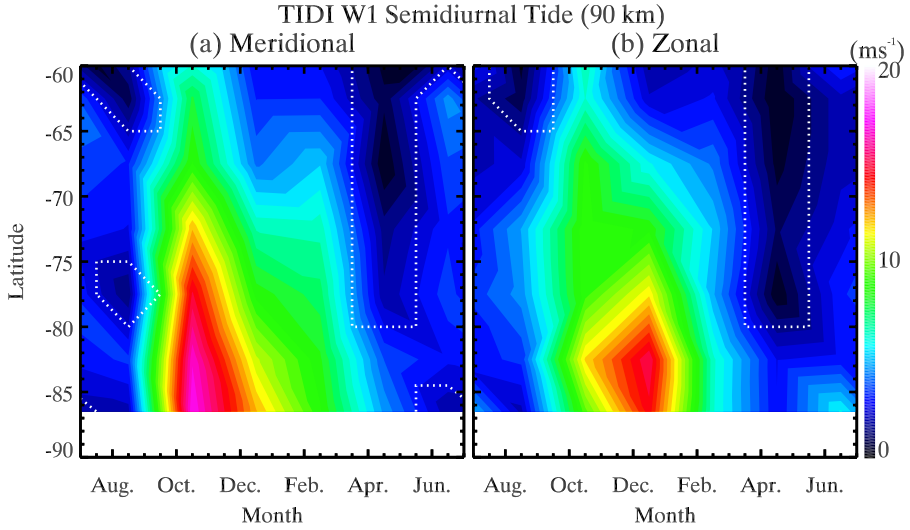

Figure 10. Seasonal variation of the W1 component as a function of latitude at 90 km. Poleward of 60°S from top to bottom is shown for (a) the meridional and (b) the zonal components. Colors range from 0 (black) to 20 (white) m s^{-1}. Amplitudes in a statistical 95% confidence interval are contoured by while dotted lines.

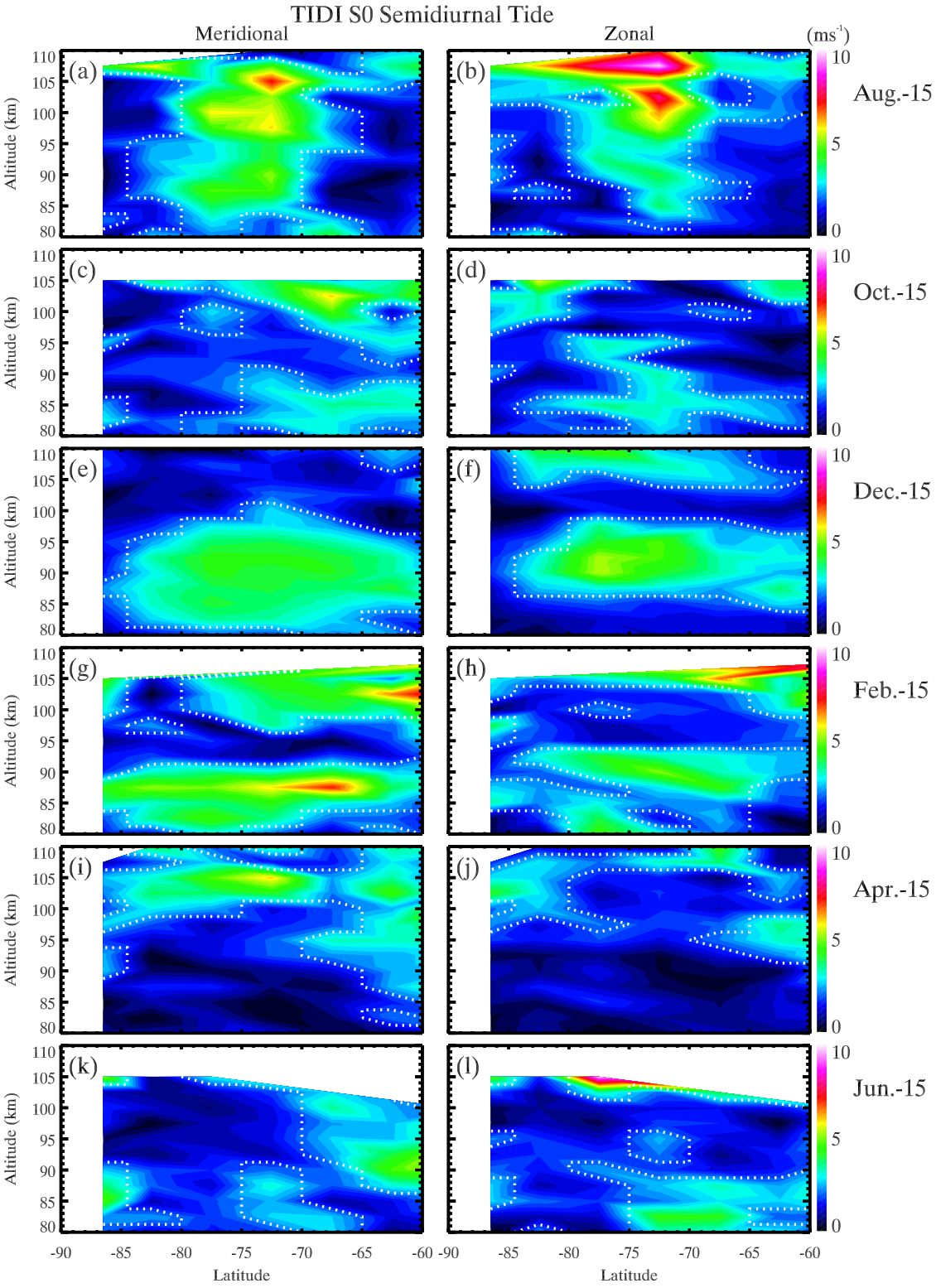

Figure 11. Spatial structure of S0 component poleward of 60°S from 80 to 110 km over six yaw periods. (a, c, e, g, i, k) Meridional component and (b, d, f, h, j, l) zonal component are shown. Dates indicate the center of the 60-day analysis window. Colors range from 0 (black) to 10 m s^{-1} (white). Amplitudes in a statistical 95% confidence interval are contoured by white dotted lines.

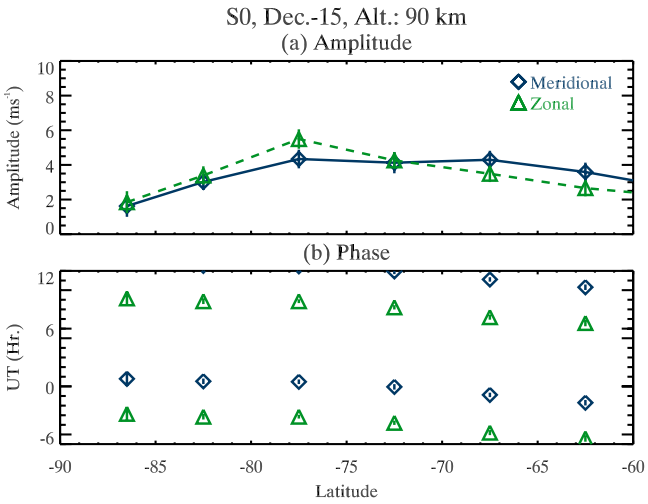

Figure 12. Latitude variations of (a) the amplitude and (b) the phase for the S0 component at 90 km from mid-November to mid-January. Blue diamonds (solid line) are for the meridional component, and green triangles (dashed line) are for the zonal component. One standard deviation from the mean value is shown as an error.

and 15 February yaw periods. During the 15 August yaw period, the S0 component maximizes in a narrow band of latitudes between 70°S and 80°S at altitudes from 85 to 105 km. During this period, the amplitude increases with altitude. The maximum amplitudes during the 15 August yaw period are located at nearly the same altitudes and latitudes between the meridional and zonal wind, with 7.4 ± 1.5 m s^{-1} at 105 km and 72.5°S in the meridional wind and 10.1 ± 2.4 m s^{-1} at 107.5 km and 72.5°S in the zonal wind. The structure of the S0 component in the meridional wind during the 15 October yaw period is very different from during the 15 August yaw period. The meridional component appears below 90 km and above 100 km and equatorward of 70°S. On the other hand, the zonal component during the 15 October yaw period appears at nearly same latitudes as during the 15 August yaw period. However, the zonal component appears below 95 km and does not increase with altitude. The meridional component during the 15 December yaw period extends to higher latitudes than during the 15 October yaw period. Therefore, the S0 component maximizes in a relatively narrow range of altitudes from 80 to 95 km and over a wide range of latitudes between 65°S and 83°S. The zonal component is very similar to the meridional component although the altitude range is narrower. The maximum amplitudes are very similar between the meridional and zonal winds, 4.4 ± 0.5 m s^{-1} at 92.5 km and 77.5°S in the meridional wind and 5.5 ± 0.6 m s^{-1} at 90 km and 77.5°S in the zonal wind. In the zonal wind, there is a second peak above 105 km and between 65°S and 85°S. The meridional component during the 15 February yaw period appears at lower altitudes in an entire latitude region between 60°S and 86.5°S. A maximum amplitude of the meridional component at 87.5 km and 67.5°S is greater than the amplitude during the 15 December yaw period. The meridional component also exists above 95 km, extending poleward of 80°S. The structure of the zonal component is reasonably similar to the meridional component. The zonal S0 component maximizes in a narrow altitude range from 90 and 95 km and a wide range of latitudes between 65°S and 82.5°S. However, the maximum amplitude of the zonal component is smaller than the meridional component. The S0 component appears mostly at higher altitudes in both meridional and zonal winds during the 15 April yaw period. However, the meridional component exhibits clearer existence than the zonal component. During the 15 June yaw period, the S0 component appears in lower latitudes in both meridional and zonal winds although the meridional component appears at higher altitudes and lower latitudes than the zonal component.

[22] Latitude variations of amplitude (Figure 12a) and phase (Figure 12b) of the S0 component at 90 km during the 15 December yaw period are shown in Figure 12. Similar latitude variations in amplitude are observed between the meridional and zonal winds. Amplitudes maximize between 67.5°S and 77.5°S. The amplitudes decrease toward lower and higher latitudes from this maximum, the decrease from 77.5°S toward 90°S is clear, and consistent with the expectation that all wind components other than the wave number 1 must approach zero at the pole [*Forbes et al.*, 1999a]. Meridional amplitude is slightly greater than the zonal amplitude equatorward of 72.5°S and smaller poleward of 72.5°S. The maximum amplitudes are 4.3 ± 0.5 m s^{-1} at 76.5°S in the meridional wind and 5.5 ± 0.6 m s^{-1} at 76.5°S in the zonal wind. Phases also exhibit clear latitude variations in both meridional and zonal winds with later phases at higher latitudes. Phase changes with latitude are at a rate of 1.0 ± 0.2 h/10° in the meridional wind and 1.2 ± 0.2 h/10° in the zonal wind. Phase difference between the meridional and zonal winds is 3.7 ± 0.1 h and is again consistent with our expectation of a 3 h time difference, with zonal component leading the meridional component.

[23] Figure 13 shows altitude variations of the amplitude and phase of the S0 component at 77.5°S from 80 to 107.5 km. The amplitudes (Figures 13a and 13c) and phases (Figures 13b and 13d) are shown during the 15 December (Figures 13a and 13b) and 15 August (Figures 13c and 13d) yaw periods. During the 15 December yaw period, the meridional component is greater than the zonal component below 90 km. The maximum difference of the amplitudes between the meridional and zonal winds occurs at 82.5 km with 2.4 ± 0.5 m s^{-1}. Altitude variations above 90 km are similar between the meridional and zonal winds, though the amplitude of the zonal component is slightly larger. The maximum amplitudes are 4.4 ± 0.5 m s^{-1} at 92.5 km in the meridional wind and 5.5 ± 0.5 m s^{-1} at 90 km in the zonal wind. Both meridional and zonal components exhibit an increase in amplitude with altitude above 102.5 km. Phase tilts in both meridional and zonal winds from 87.5 to 100 km are indicative of upward propagation. The estimated vertical wavelengths for the meridional and zonal components are 26.4 ± 1.0 km and 22.5 ± 1.2 km, respectively. Conversely, the vertical structure during the 15 August yaw period is much different from during the 15 December yaw period. During the 15 August yaw period, the amplitudes and phases show little vertical structure. The amplitudes do not show clear peaks. The much longer vertical wavelength observed during the 15 August yaw period is indicative of an evanescent wave.

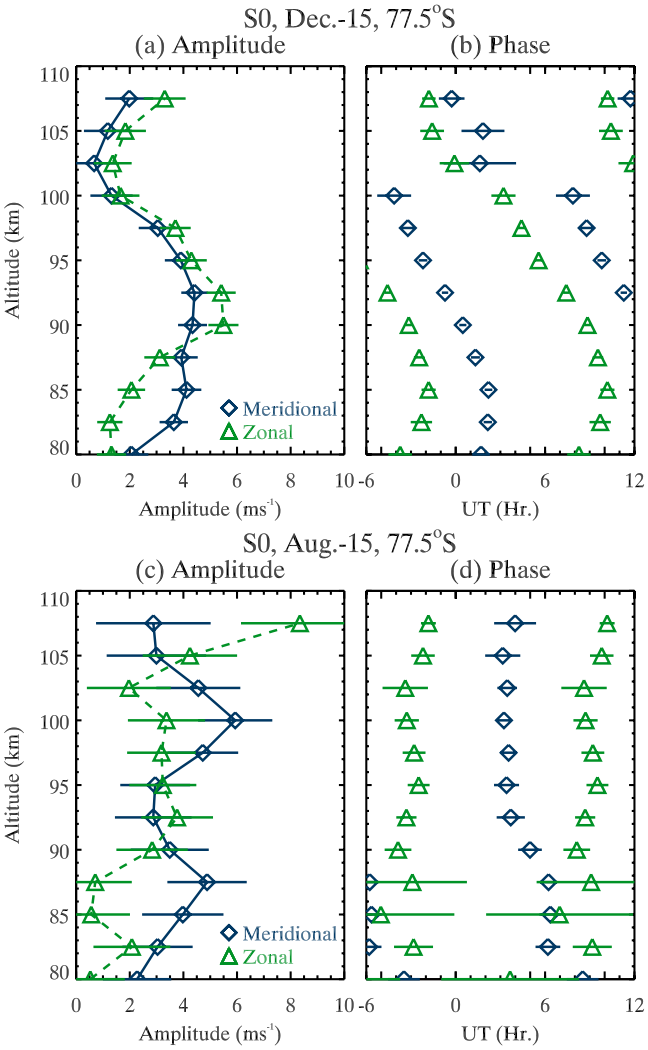

Figure 13. Altitude variations of (a, c) amplitude and (b, d) phase of the S0 component between 75°S and 80°S from mid-November to mid-January (Figures 13a and 13b) and from mid-May to mid-July (Figures 13c and 13d). Blue diamonds (solid line) and green triangles (dashed line) indicate the component in the meridional and zonal winds. One standard deviation from the mean value is shown as an error.

[24] Figure 14 shows seasonal variations of the S0 component at 90 km in the meridional (Figure 14a) and zonal (Figure 14b) winds as a function of latitude. Seasonal variations are very similar between the meridional and zonal components, maximizing between November and February, and are largely a summer phenomenon across a wide range of latitudes between 60°S and 85°S. The maximum amplitudes are 4.3 ± 0.5 m s^{-1} in the meridional wind and 5.5 ± 0.5 m s^{-1} in the zonal wind, at 77.5°S during the 15 December yaw period. The S0 component also appears during the 15 August yaw period, but in a narrower range of latitudes between 70°S and 77.5°S. The maximum amplitude at 72.5°S during the 15 August yaw period is close to the maximum amplitude during the 15 December yaw period, with 5.3 ± 1.4 m s^{-1} in the meridional wind and 4.1 ± 1.2 m s^{-1} in the zonal wind. The meridional component is greater in winter than in summer, while the zonal component is greater in summer than in winter.

3.3. Westward Propagating Zonal Wave Number 3

[25] Figure 15 is same as Figure 6 but for the W3 component. The W3 component shows reasonably similar structures between the meridional and zonal winds with larger maximum amplitudes than the S0 component throughout the year. During the 15 August yaw period, the W3 component maximizes at 72.5°S, which is the same latitude as the maximum amplitude of the S0 component. However, the W3 component maximizes below 90 km. During the 15 October yaw period, the component appears at higher altitudes in the entire latitude region between 60°S and 86.5°S. The component minimizes below 95 km during the 15 December yaw period while the amplitude of the component increases equatorward above 95 km. Therefore, at approximately 90 km where the W1 and S0 components maximize the W3 component minimizes during this period. The overall structure during the 15 February yaw period is similar to the structure during the 15 December yaw period. However, the increase in amplitude during this period starts from higher latitudes than during the 15 December yaw period. The amplitude increase during the 15 February yaw period is clearer in the meridional wind than that in the zonal wind. The maximum amplitude in the meridional wind reaches 10.1 ± 2.0 m s^{-1} at 102.5 km and 62.5°S. The overall structure during the 15 April is similar to the structures during the 15 December and 15 February yaw periods, however the amplitudes are smaller than during the 15 February yaw period and maximizes at lower altitudes than during the 15 February yaw period. The maximum amplitude is larger in the zonal wind than that in the meridional wind during this period. The zonal component maximizes at 7.7 ± 0.7 m s^{-1} at 97.5 km and 62.5°S. The structure of the W3 component is less organized during the 15 June yaw period, showing a transition to a vertically aligned and latitudinally constrained structure during the 15 August yaw period.

3.4. Eastward Propagating Zonal Wave Number 1

[26] For completeness, Figure 16 shows the spatial structure of the E1 component. There is little evidence of any significant wave activity present below 100 km throughout the year. There is an enhancement near 105 km between 60°S and 70°S during the 15 February yaw period. A somewhat weaker enhancement is also seen during the 15 June and 15 August yaw periods which extend to the highest latitudes.

3.5. Comparison With South Pole Radar Measurements

[27] The structures of the migrating and nonmigrating tides at low latitudes and midlatitudes equatorward of 45° determined from TIDI measurements have been compared with measurements from the Upper Atmosphere Research satellite (UARS) along with low-latitude and midlatitude ground-based radar and optical measurements [*Wu et al.*, 2006; *Killeen et al.*, 2006; *Oberheide et al.*, 2006; *Huang et al.*, 2006]. The tidal structures determined from the TIDI measurements are in reasonable agreement with the other

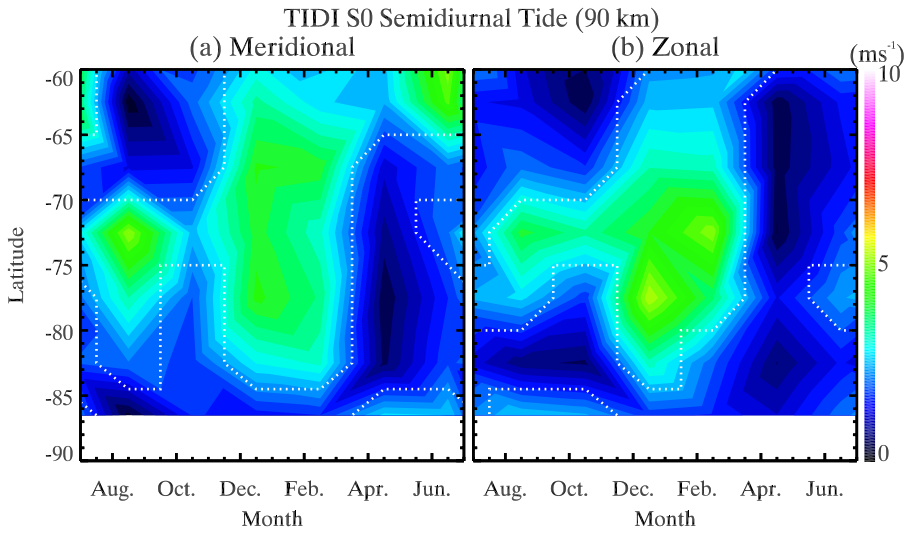

Figure 14. Seasonal variation of the S0 component as a function of latitude at 90 km. Poleward of 60°S is shown for (a) the meridional and (b) the zonal winds. Colors range from 0 (black) to 10 (white) m s^{-1}. Amplitudes in a statistical 95% confidence interval are contoured by white dotted lines.

measurements, though TIDI tidal estimates typically exhibit greater amplitudes than are reported by the ground-based measurements.

[28] One difficulty with such comparisons is the separation of the migrating and nonmigrating tidal components in the ground-based observations. This is not an issue at the South Pole because the radar system [*Forbes et al.*, 1995; *Portnyagin et al.*, 1998; *Lau et al.*, 2006] can resolve the S0, E1, and W1 components, and the zonal wave number 2 waves. As a result, it is possible to make a direct comparison between the W1 component observed at South Pole with the same component determined from the TIDI measurements. *Lau et al.* [2006] have determined the seasonal and interannual variations of the vertical profiles of the meridional W1 component in the vicinity of the South Pole using an interferometric meteor radar system. To compare the meridional W1 component determined from the TIDI and South Pole meteor radar measurements, the amplitude and phase determined from the meteor radar measurements computed for each month were averaged using a (0.25, 0.5, 0.25) weighting to replicate the yaw period sampling of the TIDI measurements. This computation results in estimated amplitudes and phases of 12.3 m s^{-1} and 5.5 h at 87.5 km and 14.5 m s^{-1} and 4.0 h at 92.5 km. During the 15 December yaw period, TIDI determined the meridional W1 component to be 11.3 m s^{-1} and 4.7 h at 87.5 km and 11.7 m s^{-1} and 2.5 h at 92.5 km. The amplitudes determined from the meteor radar measurements are slightly larger than those determined by TIDI during this period. The amplitude differences are 1.0 m s^{-1} at 87.5 km and 2.8 m s^{-1} at 92.5 km and the phase differences are 0.9 h at 87.5 km and 1.5 h at 92.5 km. One possible reason for the differences in the amplitude and phase is the difference in the altitude resolution of the two instruments. The meridional W1 component was determined with an altitude resolution of 5 km for the meteor radar system while the altitude resolution of TIDI is 2.5 km. Because TIDI observes a strong altitude variation centered at 90 km during the period from mid-November to mid-January, it is sensible that the meteor radar observes greater amplitudes at 87.5 and 92.5 km at the edge of this maximum. Additionally, the W1 component was determined from the TIDI observations at 24 longitudes using a composite day analysis spanning a 60-day yaw period while the meteor radar at the South Pole always observes the winds in four fixed longitude directions. The overall result of this comparison is the inference that the ground-based meteor radar and TIDI observations of the W1 component show very reasonable agreements in both amplitude and phase. Therefore, it is expected that the TIDI results at other altitudes and latitudes have a similar degree of fidelity.

4. Discussion

[29] Recently, *Murphy et al.* [2006] determined seasonal variations of the tidal components over Antarctica from radar wind measurements at seven locations: Scott Base (77.9°S), McMurdo (77.8°S), Halley (75.6°S), Syowa (69.0°S), Davis (68.6°S), Mawson (67.6°S), and Rothera (67.6°S). This analysis employed a simultaneous fit of data from all the radars to the Hough mode structures for all the migrating and nonmigrating tidal modes at high southern latitudes. It was assumed that amplitudes of the zonal wave number 1 components were constant with latitude while all of the other components decayed linearly to 0 at the pole. It was also assumed that the phases of all of the components were constant as a function of latitude. Our results show, in contrast, that the latitudinal structures of the nonmigrating semidiurnal components can be far more complex and can vary significantly throughout the year. Figures 6 and 7 clearly indicate that during the summer months the W1 component varies approximately linearly with latitude and decreases as one moves away from the pole. The phase of the component in both meridional and zonal winds, shown in Figure 7, changes by 2 to 3 h between the pole and 60°S. Interestingly, this phase variation is minimal poleward of 75°S and may be partially responsible for the excellent agreement in nonmigrating tidal phases found by *Portnyagin*

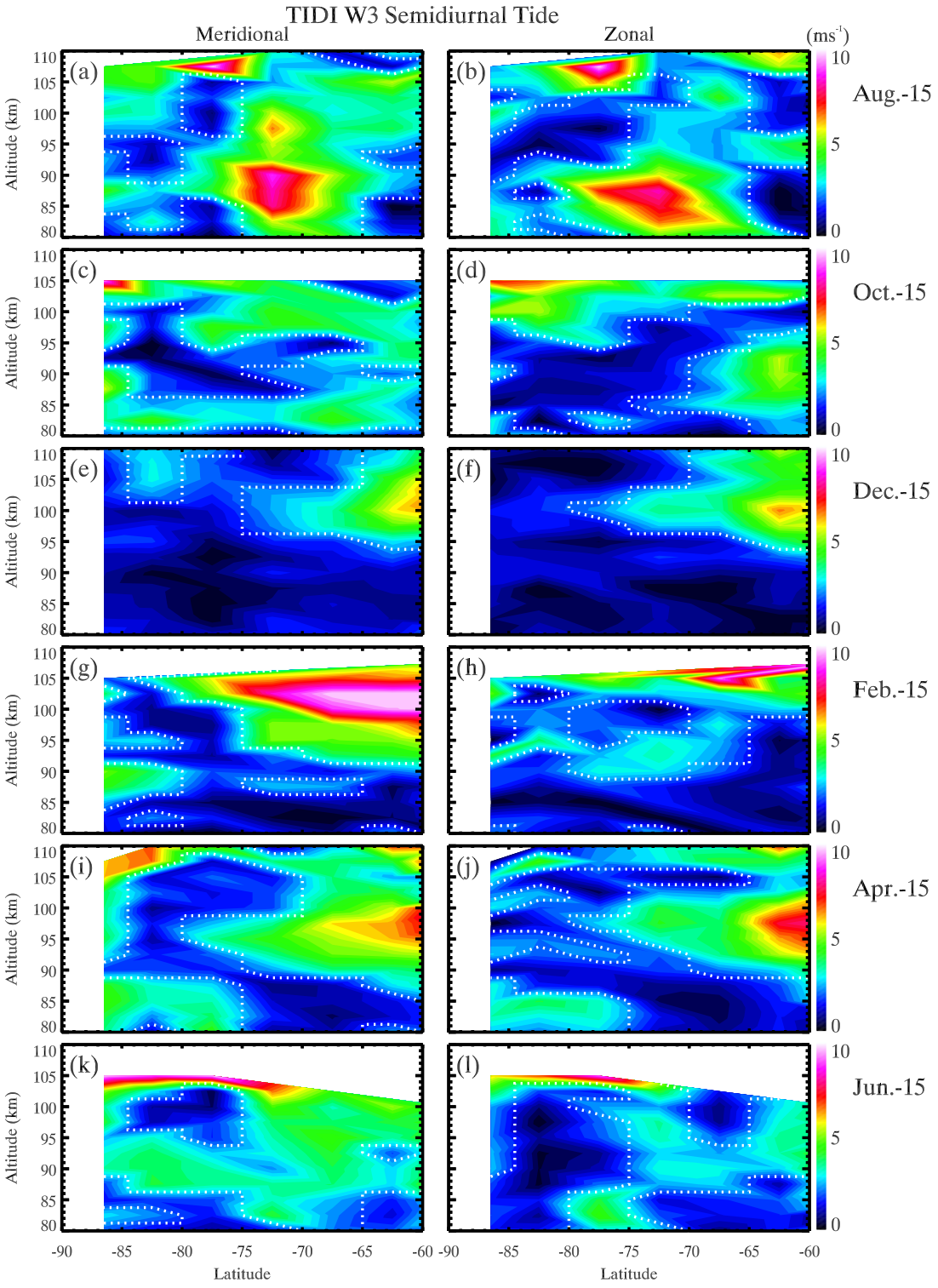

Figure 15. Spatial structure of W3 component poleward of 60°S from 80 to 110 km over six yaw periods. (a, c, e, g, i, k) Meridional component and (b, d, f, h, j, l) zonal component are shown. Dates indicate the center of the 60-day analysis window. Colors range from 0 (black) to 10 m s^{-1} (white). Amplitudes in a statistical 95% confidence interval are contoured by while dotted lines.

et al. [1998] between the South Pole and Scott Base measurements at 78°S. Additionally, both the S0 and W3 components (see Figures 11 and 15) exhibit a far more complicated latitudinal structure than a linear increase away from the South Pole. During the 15 December yaw period when the S0 component is at its maximum latitudinal extent, the amplitude structure appears to increase linearly from the pole to 77.5°S but then appears to flatten out and even

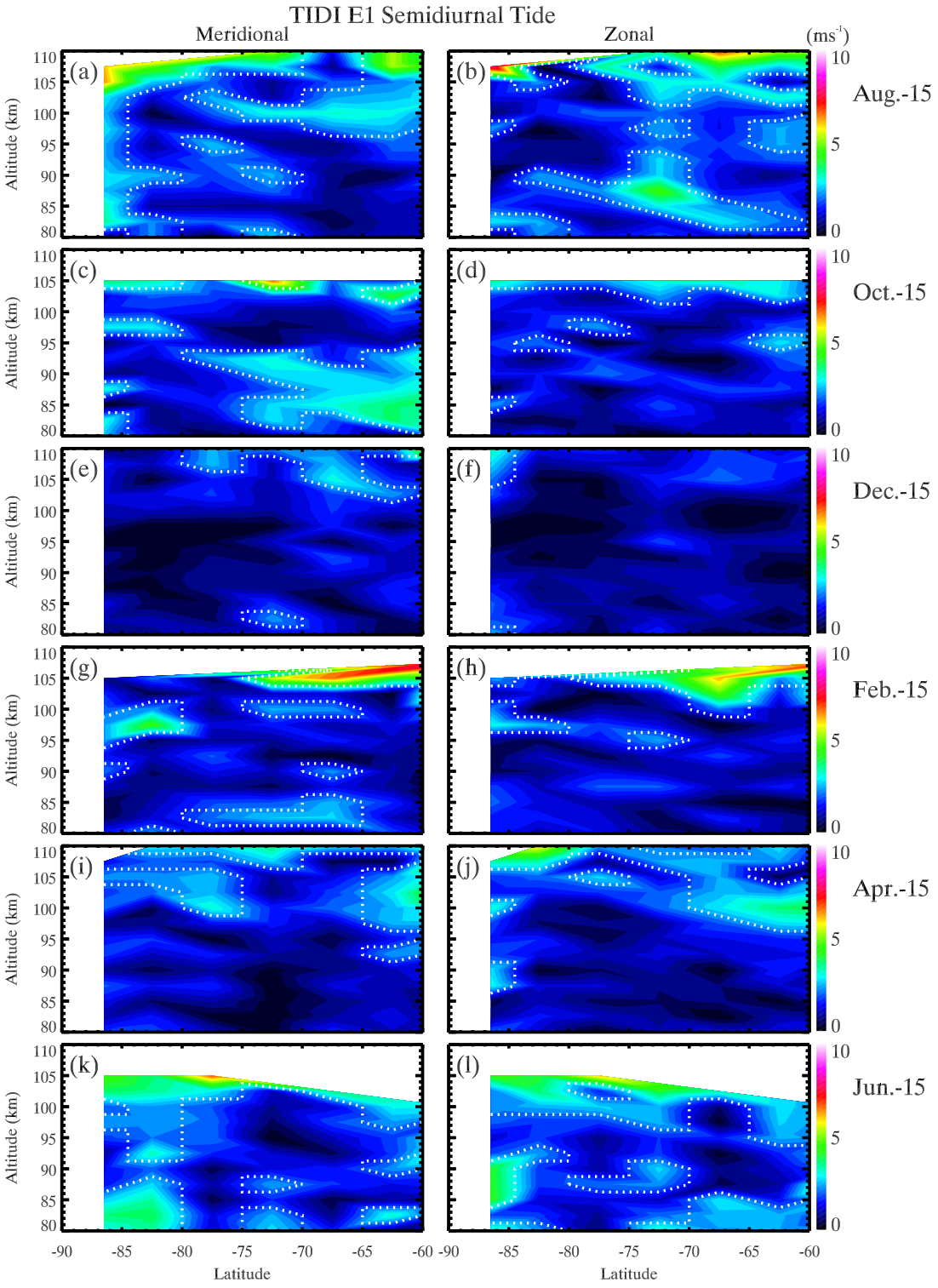

Figure 16. Spatial structure of E1 component poleward of 60°S from 80 to 110 km over six yaw periods. (a, c, e, g, i, k) Meridional component and (b, d, f, h, j, l) zonal component are shown. Dates indicate the center of the 60-day analysis window. Colors range from 0 (black) to 10 m s^{-1} (white). Amplitudes in a statistical 95% confidence interval are contoured by white dotted lines.

decrease at low latitudes. Like the W1 component, the S0 component also exhibits a slightly linear decrease in amplitude at latitudes below 75°S. Although the latitude variation of the phase of the S0 component is very similar to the W1 component, the phase of the S0 component leads the W1 component by 3 h. Therefore, the phase of the S0 component in the meridional wind is nearly same as the phase of the W1 component in the zonal wind. Although the W1 and S0 components maximize at 90 km during the 15 December yaw period, the W3 component maximizes at 100 km during

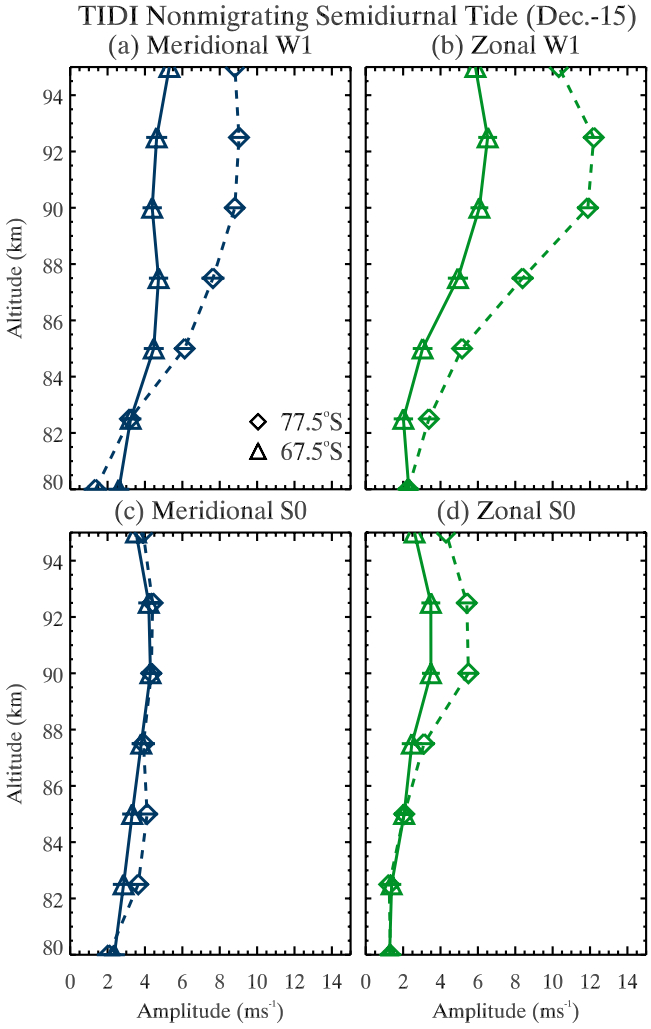

Figure 17. Altitude variations of the amplitudes of the W1 (a, b) and S0 (c, d) components in the meridional (Figures 17a and 17c) and zonal (Figures 17b and 17d) winds from mid-November to mid-January. The amplitudes at 67.5°S are shown in triangles and solid lines and at 77.5°S are shown in diamonds and dashed line.

this yaw period. In the latitude region poleward of 60°S, the maximum amplitude of the W3 component appears at 60°S. However, the amplitude of the W3 component does not increase linearly with latitude as one moves away from the pole. The amplitude of the component is nearly same poleward of 75°S and increases equatorward of 75°S.

[30] Ground-based observations of the semidiurnal tide have been made at a number of locations across the Antarctic [*Portnyagin et al.*, 1998; *Riggin et al.*, 1999; *Murphy et al.*, 2006; *Baumgaertner et al.*, 2006]. With the exception of the South Pole, all of these measurements have been made at costal Antarctic stations which are found at two latitude bands, one near 68°S and the others around 78°S. Figure 17 shows the vertical profiles of the W1 and S0 components in the meridional and zonal winds near each of these latitudes as determined from the TIDI measurements for the 15 December yaw period when both of these components exhibit significant amplitudes. In all plots the solid lines are for the latitude band centered on 67.5°S while the dashed lines are for the latitude band centered on 77.5°S. The W1 amplitudes at 77.5°S exceed the W1 amplitudes at 67.5°S over nearly all of the measurement altitudes, which clearly indicates the strong latitudinal gradient as has been previously discussed. Conversely the S0 component shows slight evidence of a latitudinal gradient in the amplitudes in the zonal wind above 85 km while the amplitudes are nearly invariant in the meridional wind.

[31] The amplitude range in the x axis and the altitude range in the y axis of Figure 17 are the same as Figure 6 of *Murphy et al.* [2006] for comparison. The amplitude of the meridional W1 component determined by *Murphy et al.* [2006] during December increases with altitude from 80 to 94 km and reaches 11.4 m s^{-1} at 94 km. This is significantly greater than 5.3 ± 0.6 m s^{-1} at 95 km determined from TIDI at 67.5°S. Although the amplitude at 77.5°S is greater than at 67.5°S from the TIDI observation, the maximum amplitude of 9.0 ± 0.5 m s^{-1} at 92.5 km and 77.5°S is smaller than 11.4 m s^{-1} at 92 km found by *Murphy et al.* [2006]. The zonal W1 component determined by *Murphy et al.* [2006] increases with altitude and the amplitude reaches 13.8 m s^{-1} at 95 km. This value is slightly larger than the amplitude of the meridional W1 component. Similar to the meridional wind, the zonal W1 component determined from TIDI increases with altitude reaching a maximum of 6.5 ± 0.5 m s^{-1} at 92.5 km and 67.5°S, which is less than half of that of *Murphy et al.* [2006]. However, TIDI observes the zonal W1 component with an amplitude of 12.2 ± 0.5 m s^{-1} at 92.5 km and 77.5°S, which is much closer to the value by *Murphy et al.* [2006]. Comparison of the S0 component during this time period again shows greater amplitudes from the ground-based determination that those determined from TIDI. The ground-based results of *Murphy et al.* [2006] show S0 amplitudes which increase with altitude and maximize near 90 km with amplitudes of 7.9 m s^{-1} in the meridional wind and 8.1 m s^{-1} in the zonal wind. In contrast, the TIDI results show a minimal vertical structure in the S0 component at 67.5°S with maximum amplitudes at 90 km with 4.3 ± 0.5 m s^{-1} in the meridional wind and 3.5 ± 0.5 m s^{-1} in the zonal wind. Although the amplitude at 77.5°S is nearly same as at 67.5°S in the meridional wind, there is a significant latitudinal variation in amplitude in the zonal wind. However, the amplitude of 5.5 ± 0.6 m s^{-1} at 90 km and 77.5°S is still smaller than by *Murphy et al.* [2006]. It is clear that there are measurable differences between the nonmigrating semidiurnal tidal determinations by TIDI and ground-based radar. These discrepancies are likely due to the assumptions of a W1 component which is invariant with respect to latitude and other components varying linearly with latitude in the ground-based analysis. At the time these were reasonable assumption however now with the TIDI measurements it is possible to unambiguously determine the spatial structure of the nonmigrating semidiurnal tides over the Antarctic. One possible future approach would be to explicitly utilize the spatial structure determined from the TIDI measurements for the ground-based analysis rather than utilizing analytic functions. A secondary factor that may play a role in these comparisons is that the ground-based radar observations were not temporally coincident with the satellite observations. According to *Murphy et al.* [2006, Table 1] the data used in the ground-based analysis

spanned from 1994 to 2004. *Baumgaertner et al.* [2005, 2006], *Portnyagin et al.* [1998], and *Riggin et al.* [1999] suggest a large interannual variation of the semidiurnal tidal amplitude from ground-based radar wind measurements in the Antarctic. If the W1 component in the vicinity of the South Pole during summer is formed by the nonlinear interaction between the migrating semidiurnal tide and stationary planetary wave zonal wave number 1 in the Northern Hemisphere, the interannual variation of the W1 component should be correlated with the migrating semidiurnal tide and stationary planetary wave. The interannual variations of the nonmigrating semidiurnal tides determined from the TIDI measurements will be discussed in future work.

[32] *Murphy et al.* [2006, Table 3] provided the estimated vertical wavelengths for each of the nonmigrating semidiurnal tidal components that was analyzed. During December, *Murphy et al.* [2006] estimated vertical wavelengths of 37 km and 33 km in the altitude region between 88 and 94 km for the meridional and zonal W1 components. This is an excellent agreement with the TIDI estimates (see Figure 8) of the vertical wavelengths for the same component during the 15 December yaw period. TIDI estimates a wavelength of the meridional W1 component between 35.0 km and 26.3 km in a latitude range between 67.5°S and 77.5°S at altitudes from 90 to 105 km. The wavelength of the zonal component is slightly shorter than the meridional component, ranging between 34.5 km and 25.3 km in the same latitude range. The difference is probably caused from the difference of the altitude range for the phase fitting. Similarly, the S0 component during December determined from ground-based analysis [*Murphy et al.*, 2006] has a vertical wavelength near 28 km in both the meridional and zonal winds which is close to 28.3 km of the mean vertical wavelength determined from TIDI between 67.5°S and 77.5°S. Additionally, *Murphy et al.* [2006] indicated that it was not possible to determine a consistent vertical wavelength for the S0 component during the winter months which is also similar to our results.

[33] During late winter of the 15 August yaw period, the S0 and W3 components show similar structures between the meridional and zonal winds, maximizing at 75°S in both components. However, the S0 component maximizes above 100 km while the W3 component maximizes below 90 km. During this period, the W1 component also reach maximum at 75°S, but above 100 km in the meridional wind and below 90 km in the zonal wind. Therefore, the nonmigrating semidiurnal tidal wind field is created mostly by the W3 component below 90 km and by a mixture of the W1 and S0 components above 100 km in the meridional wind while by a mixture of the W1 and W3 components below 90 km and by the S0 component above 100 km in the zonal wind.

[34] A slight enhancement of the E1 component is seen below 90 km in the vicinity of the pole during the 15 June yaw period. It may be related to a Lamb wave rather than the E1 semidiurnal component. *Forbes et al.* [1999a] show the presence of eastward propagating waves from South Pole meteor wind observations with periods near 12 h during the winter months. These perturbations could be responsible for the E1 enhancements observed during the 15 June yaw period.

[35] Recent modeling efforts by *Angelats i Coll and Forbes* [2002], *Yamashita et al.* [2002], and *Mayr et al.* [2005] have excited nonmigrating semidiurnal tidal signatures in mechanistic nonlinear and global circulation models. With respect to the W1 component, these models in general produce a response in the high-latitude wind field with a representative annual variation, maximizing in the summer months, but at altitudes much above what has been observed from the South Pole ground-based and TIDI measurements. As shown in Figure 6, the W1 component maximizes near or slightly below 90 km with amplitudes of 15 to 20 m s^{-1} during October through January. *Angelats i Coll and Forbes* [2002] predicted spatial structures of the semidiurnal tidal components from the nonlinear interaction theory. The structure of the meridional W1 component during January was predicted that there was not a latitudinal variations poleward of 60°S above 105 km. Although the latitudinal variation of the W1 component was seen at 100 km, the amplitude decreased poleward and was less than 4 m s^{-1} below 100 km in the vicinity of the South Pole. Figure 6 of *Angelats i Coll and Forbes* [2002] shows negligible response of the W1 component in the meridional wind below 100 km at 85°S where the TIDI and South Pole data show a large response. Figure 6 of Angelats i Coll and Forbes also exhibits a strong semiannual variation in the amplitude of the W1 component with a secondary maximum occurring in August. This structure is not present from the TIDI observations.

[36] During the yaw periods of 15 December and 15 February, TIDI observes the W3 component above 95 km. The amplitude of the W3 component during the periods increases equatorward. A structure of the W3 component by *Angelats i Coll and Forbes* [2002] shows that the amplitude of the W3 component increases equatorward and reaches 10 m s^{-1} at 110 km and 60°S. However, maximum amplitude at 100 km observed by TIDI is not predicted from the nonlinear interaction model.

[37] The results of *Yamashita et al.* [2002] using the Middle Atmosphere Circulation Model at Kyushu University (MACMKU) exhibit similar maximum amplitudes of the W1 component over the Antarctic between January and July. According to the MACMKU, the W1 component in July appears above 70 km and maximizes above 100 km at 60°S and 105 km in the vicinity of the South Pole with 15 m s^{-1}. Although TIDI observes the W1 component maximizing at 100 km poleward of 75°S from mid-July to mid-September, the maximum amplitude is less than 10 m s^{-1} and the amplitude does not increase with altitude above 80 km. The MACMKU predicts that the maximum amplitude of the W1 component in January is slightly below 110 km at 70°S and there is little evidence of the component below 100 km. Although the maximum amplitude of the W1 component predicted by the MACMKU is similar to the TIDI observations from mid-November to mid-January, the maximum amplitude from the MACMKU is located at higher altitudes than TIDI. Additionally, the MACMKU exhibits the W1 component decreasing in amplitude poleward below 105 km. The MACMKU predicts the amplitude of the W1 component with 15 m s^{-1} at 90 km and 85.8°S in August while with 10 m s^{-1} at the same altitude in February. This seasonal variation is not observed by TIDI.

The vertical wavelength of the W1 component determined by *Yamashita et al.* [2002], while not explicitly stated, is 40 km between 90 and 105 km in the vicinity of the South Pole in January. This value is much longer than the vertical wavelength determined from both the ground-based and TIDI observations.

[38] Using a numerical spectral model (NSM), *Mayr et al.* [2005] were able to reproduce tidal components. The W1 semidiurnal tidal component in the meridional wind in January and February appears above 85 km with amplitudes greater than 24 m s^{-1} in the vicinity of the South Pole. Although the amplitude by the NSM typically increases with altitude and reaches 54 m s^{-1}, the NSM predicts a small peak at 90 km. The S0 component is also predicted with a small peak at 85 km and 75°S. These structures by the NMS are similar to the TIDI observations from mid-November to mid-January. However, the amplitudes of the W1 and S0 components predicted from the NSM are much greater than the TIDI observations. Additionally, TIDI does not observe the amplitude increases in these components with altitude above 100 km. The NSM predicts the W3 component equatorward of 80°S, increasing in amplitude with altitude. The amplitude of this component is predicted as 19 m s^{-1} at 110 km and 65°S. Although the amplitude of the W3 component by the NMS is significantly greater than the TIDI observations, the structure predicted by the NMS is similar to the TIDI observations. However, TIDI does not observe the W3 component below 95 km poleward of 60°S.

5. Summary

[39] The existence of a strong W1 semidiurnal tide over the Antarctic has been known since 1993 [*Hernandez et al.*, 1993]. Measurements from the South Pole have unambiguously determined the existence and temporal evolution of this feature. Observations from ground-based sites across the Antarctic continent have previously been used in an effort to determine the spatial structure of this W1 component and to determine if other nonmigrating components exist. Furthermore, these observations have sparked a number of modeling studies focused on reproducing the W1 feature in the horizontal winds and understanding the possible mechanism underlying its existence.

[40] In this paper we have presented unambiguous determinations of the latitudinal and seasonal variation of the W1 semidiurnal tidal structure. We have also shown the existence of other nonmigrating components over the Antarctic. In particular, we have shown an evidence for the existence of the S0, W3, and a weaker E1 components over the Antarctic. The W1 component exhibits a strong annual variation with a maximum near the Austral summer solstice in the meridional wind. This is consistent with the previous South Pole results. A more detailed comparison between the TIDI and South Pole meteor results during the 15 December yaw period shows excellent agreement between the measurements with differences less than a few meters per second, indicating high confidence in the TIDI results.

[41] While the meridional W1 component maximizes before the Austral summer solstice the zonal W1 component maximizes near the solstice. Because the South Pole observations only measure meridional winds, this feature was previously unknown. Between equinox and solstice when the W1 component maximizes the peak amplitudes of 15 to 20 m s^{-1} are observed in a stratified layer near 90 km which spans the Antarctic from the pole to 60°S and decreases equatorward. After the solstice the W1 component evolves into a bifurcated structure with a lower peak at 85 km and an upper peak at 100 km which are both expansive in latitude. The vertical wavelengths computed for the W1 component are consistent in both meridional and zonal winds and increase equatorward from near 20 km at the pole to over 40 km at 60°S.

[42] A significant S0 component was also observed by TIDI. This component appears around both the summer and winter solstice in both meridional and zonal winds. However, the spatial structure of the S0 component changes between seasons. During the winter solstice the S0 component is confined to a narrow band of latitude but spans the altitude range from 80 to 110 km. Conversely during the summer solstice the S0 component is horizontally stratified similar to the W1 component spanning a broad range of latitudes. The vertical wavelengths of this component change dramatically from near 25 km in the summer to nearly evanescent during the winter.

[43] Evidence of a significant W3 component was also indicated throughout the year from the observations. This component achieves amplitudes nearing 10 m s^{-1} equatorward of 75°S and decreases in amplitude toward the pole. The largest amplitudes occur during the late summer and the winter. During late summer the W3 component appears stratified in altitude similar to the W1 and S0 components while the W3 component maximizes at higher altitudes than the W1 and S0 components. The structure of the W3 component is less stratified and more latitudinally constrained during late winter similar to the S0 component. However, the W3 component during late winter maximizes at lower altitudes than the S0 component.

[44] Comparisons of the TIDI observations with model results indicate that current nonlinear models cannot accurately represent the vertical amplitude or phase structure of the W1 component. Such model results are important in developing a full understanding of the mechanisms which generate the nonmigrating semidiurnal tide. It is expected that the results presented here provide a new understanding of the structure of the nonmigrating semidiurnal tides which have not previously been observed and will aid in furthering our understanding of these phenomena.

[45] **Acknowledgments.** A basic concept of the nonmigrating tidal analyses in the high-latitude region by the TIDI measurements is from the tidal analyses of the SABER temperature measurements by J. M. Forbes. We thank D. C. Fritts and D. M. Riggin for their helpful and insightful comments. This work has been supported by the National Science Foundation Office of Polar Programs grant ANT0538672 and by OPP-0438777. The TIDI work at NCAR and CoRA is supported by NASA grants NXX07AB76G, NNH05CC70C, and NNH05CC69C.

References

Angelats i Coll, M., and J. M. Forbes (2002), Nonlinear interactions in the upper atmosphere: The s = 1 and s = 3 nonmigrating semidiurnal tides, *J. Geophys. Res.*, *107*(A8), 1157, doi:10.1029/2001JA900179.

Baumgaertner, A. J. G., A. J. McDonald, G. J. Fraser, and G. E. Plank (2005), Long-term observations of mean winds and tides in the upper mesosphere and lower thermosphere above Scott Base, Antarctica, *J. Atmos. Sol. Terr. Phys.*, *67*, 1480–1496, doi:10.1016/j.jastp.2005.07.018.

Baumgaertner, A. J. G., M. J. Jarvis, A. J. McDonald, and G. J. Fraser (2006), Observations of the wavenumber 1 and 2 components of the semi-diurnal tide over Antarctica, *J. Atmos. Terr. Phys.*, *68*, 1195–1214, doi:10.1016/j.jastp.2006.03.001.

Burrage, M. D., D. L. Wu, W. R. Skinner, D. A. Ortland, and P. B. Hays (1995), Latitude and seasonal dependence of the semidiurnal tide observed by the high resolution Doppler imager, *J. Geophys. Res.*, *100*, 11,313–11,322, doi:10.1029/95JD00696.

Chapman, S., and R. Lindzen (1970), *Atmospheric Tides: Thermal and Gravitational*, D. Reidel, Dordrecht, Netherlands.

Du, J., W. E. Ward, J. Oberheide, T. Nakamura, and T. Tsuda (2007), Semidiurnal tides from the extended Canadian Middle Atmosphere Model (CMAM) and comparisons with TIMED Doppler Interferometer (TIDI) and meteor radar observations, *J. Atmos. Sol. Terr. Phys.*, *69*, 2159–2202, doi:10.1016/j.jastp.2007.07.014.

Forbes, J. M. (1995), Tidal and planetary waves, in *The Upper Mesosphere and Lower Thermosphere: A Review of Experiment and Theory*, *Geophys. Monogr. Ser.*, vol. 87, edited by R. M. Johnson and T. L. Killeen, pp. 67–87, AGU, Washington, D. C.

Forbes, J. M., and H. B. Garrett (1979), Theoretical studies of atmospheric tides, *Rev. Geophys. Space Phys.*, *17*, 1951–1981.

Forbes, J. M., N. A. Makarov, and Y. I. Portnyagin (1995), First results from the meteor radar at South Pole: A large 12-hour oscillation with zonal wavenumber one, *Geophys. Res. Lett.*, *22*, 3247–3250, doi:10.1029/95GL03370.

Forbes, J. M., S. E. Palo, X. Zhang, Y. I. Portnyagin, N. A. Makarov, and E. G. Merzlyakov (1999a), Lamb waves in the lower thermosphere: Observational evidence and global consequences, *J. Geophys. Res.*, *104*, 17107–17116, doi:10.1029/1999JA900044.

Forbes, J. M., I. Y. Portnyagin, N. A. Makarov, S. E. Palo, E. G. Merzlyakov, and X. Zhang (1999b), Dynamics of the lower thermosphere over South Pole from meteor radar wind measurements, *Earth Planets Space*, *51*, 611–620.

Fritts, D. C., and J. R. Isler (1994), Mean Motions and Tidal and Two-Day Structure and Variability in the Mesosphere and Lower Thermosphere over Hawaii, *J. Atmos. Sci.*, *51*, 2145–2164.

Hernandez, G., G. J. Fraser, and R. W. Smith (1993), Mesospheric 12-hour oscillation near South Pole, Antarctica, *Geophys. Res. Lett.*, *20*, 1787–1790, doi:10.1029/93GL01983.

Huang, F. T., H. G. Mayr, C. A. Reber, T. Killeen, J. Russell, M. Mlynczak, W. Skinner, and J. Mengel (2006), Diurnal variations of temperature and winds inferred from TIMED and UARS measurements, *J. Geophys. Res.* (Space Physics), *111*, A10S04, doi:10.1029/2005JA011426.

Kato, S., T. Tsuda, and F. Watanabe (1982), Thermal excitation of non-migrating tides, *J. Atmos. Terr. Phys.*, *44*, 131–146.

Killeen, T. L., et al. (1999), TIMED Doppler interferometer (TIDI), in *Optical Spectroscopic Techniques and Instrumentation for Atmospheric and Space Research III*, edited by A. M. Larar, *Proc. SPIE*, *3756*, 289–301.

Killeen, T. L., Q. Wu, S. C. Solomon, D. A. Ortland, W. R. Skinner, R. J. Niciejewski, and D. A. Gell (2006), TIMED Doppler Interferometer: Overview and recent results, *J. Geophys. Res.*, *111*, A10S01, doi:10.1029/2005JA011484.

Lau, E. M., S. K. Avery, J. P. Avery, S. E. Palo, and N. A. Makarov (2006), Tidal analysis of meridional winds at the South Pole using a VHF interferometric meteor radar, *J. Geophys. Res.*, *111*, D16108, doi:10.1029/2005JD006734.

Lindzen, R. S. (1978), Effects of daily variations of cumulonimbus activity on the atmospheric semidiurnal tide, *Mon. Weather Rev.*, *106*, 526–533.

Mayr, H. G., J. G. Mengel, E. R. Talaat, H. S. Porter, and K. L. Chan (2005), Mesopsheric non-migrating tides generated with planetary waves: I. Characteristics, *J. Atmos. Sol. Terr. Phys.*, *67*, 959–980.

McLandress, C., Y. Rochon, G. G. Sheperd, B. H. Solheim, G. Thuillier, and F. Vial (1994), The meridional wind component of the thermospheric tide observed by WINDII on UARS, *Geophys. Res. Lett.*, *21*, 2417–2420.

Murphy, D. J., et al. (2006), A climatology of tides in the Antarctic mesosphere and lower thermosphere, *J. Geophys. Res.*, *111*, D23104, doi:10.1029/2005JD006803.

Oberheide, J., Q. Wu, T. L. Killeen, M. E. Hagan, and R. G. Roble (2006), Diurnal nonmigrating tides from TIMED Doppler Interferometer wind data: Monthly climatologies and seasonal variations, *J. Geophys. Res.*, *111*, A10S03, doi:10.1029/2005JA011491.

Oberheide, J., Q. Wu, T. L. Killeen, M. E. Hagan, and R. G. Roble (2007), A climatology of nonmigrating semidiurnal tides from TIMED Doppler Interferometer (TIDI) wind data, *J. Atmos. Sol. Terr. Phys.*, *69*, 2203–2218, doi:10.1016/j.jastp.2007.05.010.

Palo, S. E., Y. I. Portnyagin, J. M. Forbes, N. A. Makarov, and E. G. Merzlyakov (1998), Transient eastward-propagating long-period waves observed over the South Pole, *Ann. Geophys.*, *16*, 1486–1500.

Portnyagin, Y. I., et al. (1994), The wind regime of the mesosphere and lower thermosphere during the DYANA campaign - II. Semi-diurnal tide, *J. Atmos. Terr. Phys.*, *56*, 1731–1752.

Portnyagin, Y. I., J. M. Forbes, N. A. Makarov, E. G. Merzlyakov, and S. Palo (1998), The summertime 12-h wind oscillation with zonal wavenumber s = 1 in the lower thermosphere over the South Pole, *Ann. Geophys.*, *16*, 828–837.

Riggin, D. M., D. C. Fritts, M. J. Jarvis, and G. O. L. Jones (1999), Spatial structure of the 12-hour wave in the Antarctic as observed by radar, *Earth Planets Space*, *51*, 621–628.

Skinner, W. R., et al. (2003), Operational performance of the TIMED Doppler Interferometer (TIDI), *Optical Spectroscopic Techniques and Instrumentation for Atmospheric and Space Research V*, edited by A. M. Larar, J. A. Shaw, and Z. Sun, *Proc. SPIE*, *5157*, 47–57, doi:10.1117/12.503727.

Teitelbaum, H., and F. Vial (1991), On tidal variability induced by nonlinear interaction with planetary waves, *J. Geophys. Res.*, *96*, 14,169–14,178.

Wu, Q., T. L. Killeen, D. A. Ortland, S. C. Solomon, R. D. Gablehouse, R. M. Johnson, W. R. Skinner, R. J. Niciejewski, and S. J. Franke (2006), TIMED Doppler interferometer (TIDI) observations of migrating diurnal and semidiurnal tides, *J. Atmos. Terr. Phys.*, *68*, 408–417, doi:10.1016/j.jastp.2005.02.031.

Yamashita, K., S. Miyahara, Y. Miyoshi, K. Kawano, and J. Ninomiya (2002), Seasonal variation of non-migrating semidiurnal tide in the polar MLT region in a general circulation model, *J. Atmos. Sol. Terr. Phys.*, *64*, 1083–1094.

Yee, J.-H., G. E. Cameron, and D. Y. Kusnierkiewicz (1999), Overview of TIMED, in *Optical Spectroscopic Techniques and Instrumentation for Atmospheric and Space Research III*, edited by A. M. Larar, *Proc. SPIE*, *3756*, 244–254.

H. Iimura, Colorado Research Associates, 3380 Mitchell Lane, Boulder, CO 80303, USA. (iimurah@cora.nwra.com)

T. L. Killeen, S. C. Solomon, and Q. Wu, National Center for Atmospheric Research, High Latitude Observatory, P.O. Box 3000, Boulder, CO 80307-3000, USA.

S. E. Palo, Department of Aerospace Engineering Sciences, University of Colorado, 429 UCB, Boulder, CO 80309, USA.

W. R. Skinner, Space Physics Research Laboratory, University of Michigan, Space Research Building, 2455 Hayward Street, Ann Arbor, MI 48109-2143, USA.